FULL ARTICLE

Colon cancer detection by using Poincaré sphere and 2D polarimetric mapping of *ex vivo* colon samples

Deyan Ivanov*[1] | Viktor Dremin[2,3] | Alexander Bykov[3] | Ekaterina Borisova[1,4] | Tsanislava Genova[1] | Alexey Popov[5] | Razvigor Ossikovski[6] | Tatiana Novikova[6] | Igor Meglinski[3,7,8,9,10]

[1]Institute of Electronics, Bulgarian Academy of Sciences, Sofia, Bulgaria
[2]Research & Development Center of Biomedical Photonics, Orel State University, Orel, Russia
[3]Optoelectronics and Measurement Techniques unit, University of Oulu, Oulu, Finland
[4]Biology Faculty, Saratov State University, Saratov, Russia
[5]VTT Technical Research Centre of Finland, Oulu, Finland
[6]LPICM, Ecole Polytechnique, Palaiseau, France
[7]Interdisciplinary Laboratory of Biophotonics, National Research Tomsk State University, Tomsk, Russia
[8]Institute of Engineering Physics for Biomedicine (PhysBio), National Research Nuclear University - MEPhI, Moscow, Russia
[9]School of Engineering and Applied Science, Aston University, Birmingham, UK
[10]School of Life and Health Sciences, Aston University, Birmingham, UK

Correspondence
*Deyan Ivanov Email: d.ivanov@ie.bas.bg

Present Address
72, Tsarigradsko chaussee blv., Sofia, Bulgaria

This work is dedicated to the diagnosis and grading of colon cancer by a combined use of Poincaré sphere and 2D Stokes vector polarimetry mapping approaches. The major challenge consists in exploring the applicability of polarized light for non-invasive screening of the histological abnormalities within the samples of biological tissues. Experimental studies were conducted in *ex vivo* colon sample, excised after surgical procedure for colon tumour removal of G2-adenocarcinoma lesion. Polarimetric measurements in linear and circular regime were carried via personally developed polarimetric, optical set-up, using supercontinuous fibre laser with irradiation fixed at 635 nm. We apply the Poincaré sphere and two-dimensional Stokes vector scanning approach for screening the corresponding tissue samples. A comparison between linear and circular polarization states is made both for quantitative and qualitative evaluations. It is shown that circular polarization has better diagnostic capabilities than linear polarization, with higher dynamic ranges of the polarimetric parameters and better values of the diagnostic quantities. In addition to the standard polarimetry parameters, utilized as essential diagnostic markers, we apply statistical analysis to obtain more detailed information in frame of the applied diagnostic approach.

KEYWORDS:

Tissue diagnostics, Stokes polarimetry, Polarimetric mapping, *Poincaré* sphere, Colon cancer

1 | INTRODUCTION

Beyond any doubt, both early cancer detection and targeted therapy aim to increase life expectancy and to improve quality of life among patients. The *Global Cancer Observatory* provides rich statistical database, regarding cancer caused by different types of viruses, as well as health issues.[1] Colon cancer is one of the leading cases of malignancy and, unfortunately, due to its anatomical origins it is often diagnosed at later stage of development. Gastrointestinal tumors are responsible for high mortality rate (nearly 9 mortality cases from 20 initial diagnosis, according to the *Global Caner Observatory*), especially when late, little or no screening has been applied.[1,2] In general, colon cancer stages can be classified as: *i)* morphological and biochemical alterations in the epithelium cells, with additional cellular density growth; *ii)* invasion of tumors cells into the adjacent tissue, which leads to the destruction of the healthy tissue; *iii)* metastasis as a result of the tumor spread in other locations of body via the lymph or the

blood.[3] Pathologists are responsible for conducting macroscopic and microscopic examinations of resected tissues from surgery. These types of examinations are aiming to make accurate diagnosis and to localize any zones of the tissues with residual cancer.[4] However, this is not a trivial task, requiring extensive knowledge and experience, time consuming, involving sample cutting and fixing, with possible tissue staining with hematoxylin and eosin, as well as preparation and examination of many histological slides.[5,6] The aforementioned alterations, when tumors are growing *(i-iii)*, are inevitably related to changes in the optical properties of the tissues under examination, namely: the scattering and the absorption coefficients μ_s, μ_a; the anisotropy factor g; as well as the refractive index n.[7] Therefore, optical methods and techniques may provide supplementary diagnostic information for pathologists, with high sensitivity. Moreover, they are fast and relatively cheap to acquire, with minimal invasiveness.[8,9] Such non-invasive and fast evaluation of the tissue state for development of an "optical biopsy" – based diagnosis could be a significant improvement of the current diagnostic modalities used in laboratorial and clinical practice. Different optical modalities are applied for primary detection and diagnosis of gastrointestinal cancerous lesions, such as fluorescence detection with and without exogenous fluorescent markers applied,[10–12] diffuse-reflectance,[13] Raman[14] and NIR[15] spectroscopy. Spectroscopic techniques allow to obtain biochemical and morphological information about the investigated tissue. Optical coherence tomography technique is also applied for gastrointestinal mucosa diagnosis, but principal information that could be obtained is morphological alterations observed during tumour growth.[16] All of these techniques, used solely or in combination, could enrich the information obtained from the tissue under investigation, allowing improvement of the diagnostic abilities and accuracy achieved.[16,17] Usually endoscopic instruments are combined with the practical techniques mentioned above and upgraded with spectral detection probes or imaging channels to evaluate the suspicious tissue areas.[18] The most recent developments combine wireless capsule endoscopy technique with spectroscopic detection of GI tumours as well.[19] Tissue polarimetry, for example, is widely used as a diagnostic tool where healthy and tumorous tissue samples modify the initial state of polarization or decrease the initial degree of polarization.[20–28] Mueller matrices of the corresponding tissue specimens under examination can give insight of their polarization-depolarization properties.[29] Polarimetric imaging possesses tremendous advantages, in order to localize small, but significant histological alteration within the examined or scanned tissue zone.[4,30–32] In this paper, we present a diagnostic approach for quantitative evaluation of the polarization changes, resulting from histological abnormalities, associated with cancer, by using the Poincaré

sphere as a graphical tool[33–36]. An evaluation of the sensitivity, specificity and accuracy of diagnostics with regard to the polarimetric method is made, as well as detailed statistical analysis. Finally, polarimetric, comparative results from two-dimensional scanning of different histological sample sections are provided.

2 | MATERIALS AND METHODS

2.1 | Theory

2.1.1 | Polarimetric quantities

The polarization states of light with arbitrary degrees of polarization can be described in terms of the Stokes formalism:[37,38]

$$
\begin{bmatrix} S_0 \\ S_1 \\ S_2 \\ S_3 \end{bmatrix} = \begin{bmatrix} I_H + I_V \\ I_H - I_V \\ I_P - I_M \\ I_{RCP} - I_{LCP} \end{bmatrix}, \tag{1}
$$

where I stands for light intensity, the subscripts indicate light polarization, i.e.: H – horizontal, V – vertical, P/M – $\pm 45°$ and RCP/LCP are the right and left circular polarizations, respectively. From these parameters, other polarimetric quantities, such as ellipticity – ϵ and azimuth – θ angles, alongside the total degree of polarization (DOP) and/or the linear/circular DOPs can be expressed as:[38]

$$
\epsilon = \frac{1}{2}\sin^{-1}\left(\frac{S_3}{\sqrt{S_1{}^2 + S_2{}^2 + S_3{}^2}}\right); \ -\frac{\pi}{4} \leq \epsilon \leq \frac{\pi}{4}. \tag{2}
$$

$$
\theta = \frac{1}{2}\tan^{-1}\left(\frac{S_2}{S_1}\right); \ -\frac{\pi}{2} \leq \theta \leq \frac{\pi}{2}. \tag{3}
$$

$$
DOP = \frac{\sqrt{S_1{}^2 + S_2{}^2 + S_3{}^2}}{S_0}; \ 0 \leq DOP \leq 1. \tag{4a}
$$

$$
DOLP = \frac{\sqrt{S_1{}^2 + S_2{}^2}}{S_0}; \ 0 \leq DOLP \leq 1. \tag{4b}
$$

$$
DOCP = \frac{|S_3|}{S_0}; \ 0 \leq DOCP \leq 1. \tag{4c}
$$

When polarized light travels into biotissues, which are anisotropic and non-homogeneous optical media, due to multiple scattering events a change of the initial polarization state and a decrease of the degree of polarization take place. Any polarization change can be described qualitatively via the Poincaré sphere and quantitatively by the parameters ϵ

and θ. Again, qualitatively any depolarization can be visualized, depending on the position within the Poincaré sphere and quantitatively by the parameters of DOP. Now, suppose we have three dimensional Cartesian coordinate system in which the axes are the Stokes parameters S_1, S_2 and S_3, normalized by S_0. Placing the origin of the coordinate system at the center of unit sphere and applying the spherical transformation of the Cartesian coordinates, we can relate the aforementioned quantities to the Poincaré sphere as follows: [39]

$$\begin{bmatrix} S_0 \\ S_1 \\ S_2 \\ S_3 \end{bmatrix} = DOP \begin{bmatrix} \frac{1}{DOP} \\ cos(2\epsilon)cos(2\theta) \\ cos(2\epsilon)sin(2\theta) \\ sin(2\epsilon) \end{bmatrix}. \tag{5}$$

2.1.2 | Diagnostic quantities

Results originating from different diagnostic tests other than histological ones should lead to conclusions identical to those derived from the "Gold Standard" set by histology. In this paper we compared the results from pathologists, considered as reference, and those from polarimetric experiments. Therefore, for this particular reason, several diagnostic quantities have been implemented: [40] Sensitivity, Specificity, Accuracy, Positive/Negative Predictive Values (PPV/NPV), Index of Suspicion (IS) and Threat Score (TS) all of which are defined via the concept of True Positive/Negative and False Positive/Negative values, denoted correspondingly as TP, TN, FP and FN:

$$\text{Sensitivity} = \frac{\text{TP}}{\text{TP+FN}}, \quad \text{Specificity} = \frac{\text{TN}}{\text{TN+FP}}, \tag{6a}$$

$$\text{Accuracy} = \frac{\text{TP+TN}}{\text{TP+TN+FP+FN}}, \tag{6b}$$

$$\text{PPV} = \frac{\text{TP}}{\text{TP+FP}}, \quad \text{NPV} = \frac{\text{TN}}{\text{TN+FN}}, \tag{6c}$$

$$\text{IS} = \frac{\text{TP+FP}}{\text{TP+FN}}, \quad \text{TS} = \frac{\text{TP}}{\text{TP+FN+FP}}, \tag{6d}$$

For better clarity, TP represents histological zone of the tissue under examination, classified as malignant by histology and polarimetry. Analogously, TN is evaluation by both methods as healthy zone. FP is histologically diagnosed tissue as normal and malignant with polarimetry and finally, FN is histologically diagnosed tissue as malignant, but healthy with polarimetry. The above-mentioned diagnostic quantities can be of great help, in order to have feedback of how accurate and effective diagnostics can be performed by our method, in comparison with the "Gold Standart".

2.2 | Sample specifications

In this paper, the results are from experiments with *ex vivo* colon sample, obtained from patient's operation, containing one of the most common tumor in the colon – G2-Adenocarcinoma. The biological specimen was provided after excision and Pathologist's diagnosis from University Hospital Tzaritza Yoanna-ISUL. The tissue sample used in the current study was selected knowledgeably without inclusion criteria, such as: age, gender of the patient and etc., except evaluated presence of colon adenocarcinoma in second grade of development, which allowed us to observed a significant state of tumour growth, but before appearance of metastatic activity and necrotic areas in the lesion investigated. All regulations from the ethical committee of the hospital have been passed. The sample itself consists of two sections - one healthy and one tumor and the origins of the measurements were marked in Fig. 1.
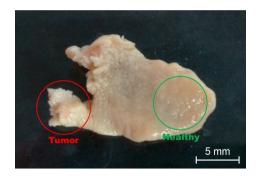

FIGURE 1 *Ex vivo* colon sample with its corresponding ROIs.

The thicknesses of both sections are several millimeters and such depth requires usage of reflection geometry for the experiments. No additional staining and contrast agents were used. Before conducting any of the measurements, the sample was stored in formalin. Both the colon sample histological sections, used as reference from the physicians, were scanned with region of interest (ROI) 1 mm × 1mm and a step size of 0.2 mm. Including the zeroth co-ordinates of both axes, 36 measurements from both ROIs were acquired. The points were chosen arbitrary, satisfying the condition to be within the histological zones, marked from the physicians.

2.3 | Experimental set-up

The experimental setup used consists of two major parts: polarization state generation (PSG, Fig. 2a) and polarization state detection (PSD, Fig. 2b).
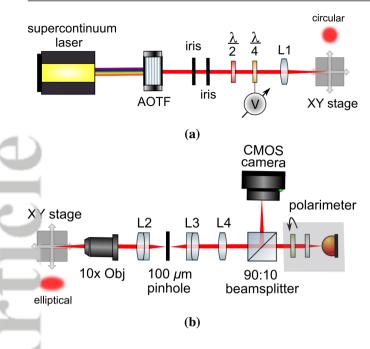
FIGURE 2 Schematic representation of the experimental set-up: a) polarization state generation channel and b) polarization state detection channel. For better clarity, only top view is shown.

PSG is at 55° with respect to the normal of the colon sample. The rest of the PSG comprises: a supercontinuum fiber laser (Leukos Ltd., France), connected to an acousto-optic tunable filter (Leukos Ltd., France) by which a wavelength 635 nm with a spectral width of 8 nm is acquired, by this way conforming our measurements to the spectral gap, where the scattering dominates over absorption in tissues and the length is detectable with the polarimetric device; two consequently placed and aligned irises, assuring parallel beam; The light emerging from the filter is linearly polarized, altered by a half-wave plate into desired state of linear polarization and a liquid crystal voltage-variable quarter-wave plate assures circular polarization respectively; a lens L_1 focuses the light beam on the sample under examination, positioned on a motorized xy stage with manual control of the z axes. The output power is 2 mW. With respect to the sample, PSD is at 30° and comprises: an objective lenses with $10\times$ magnification; a lenses L_2 alongside with 100 μm pinhole and a L_3 aiming to exclude any achromatic abberations; another lens focuses the light on a 90-10 beam splitter; the reflected light enters a CMOS camera for precise focus adjustment, while the transmitted light enters the polarimetric device (Thorlabs Ltd., USA) where a rotating quarter-wave plate and a fixed linear polarizer modulate periodically the light reflected from the sample, before reaching the photo detector – Si photodiode. The results are presented in the following section.

2.4 | Statistical analysis

By using various statistical tests, valuable and supplementary information for diagnostics can be extracted. For this particular reason, the experimental data needs to be properly selected, by separate division of the obtained results into two major groups, each for the two input polarization states used for scanning (H & RCP). Thereafter, the Stokes parameters can be plotted on the Poincaré sphere, so that each locus on the sphere will represent particular polarization state. All loci can be assigned with their corresponding coordinates, namely: S_1, S_2 and S_3. Consequently, the diagnostic quantities can be calculated, where it is expected *a priori* to have different diagnostic quantities for both polarizations states used. All tests ought to be conducted once for the group of circular polarization measurements and once for the group of linear polarization measurements, where in both cases the desired aims are intended to extract information, whether there is significant difference between the various group values and if they are drawn from the same population. Taking into account the relatively small sample sizes, nonparametric tests were used to confirm the reliability of differences independently between the groups. Namely, the test are: Mann-Whitney U and Kruskal-Wallis with additional *post-hoc* analysis via the pairwise Tukey's test. The evaluation of the results was considered as statistically significant if $p<\alpha$, where p is the calculated value for each test and α is the significance level. All tests were computed via R language and environment for statistics [41] on a significance level 0.05.

3 | RESULTS AND DISCUSSION

3.1 | Poincaré sphere as a graphical tool

In Fig.3, coordinates of each point on the Poincaré sphere represents the Stokes parameters, measured with the polarization-based experimental system described in the previous section. It should be pointed out here that this representation does not include corrections for DOP. Therefore, all the points can be seen on the surface of the Poincaré sphere, whereas utilizing these corrections the points would have been inside the sphere closer to its origin [42]. It has been reported earlier, that for Mie scattering (when scattering is dominated by large spherical particles with a diameter greater than wavelength of incident laser light) the circularly polarized light preserves its helicity during the larger amount of scattering events, known as a polarization memory. [43–46] Linear polarization possesses no such sense of the directional awareness towards propagation of light and it is not able to maintain its polarizing properties well for a large number of scattering events. Therefore, this phenomenon ensures a larger penetration depth without depolarization for circularly polarized light compared to the one of linearly polarized light. [33,36,47,48] In the current study, we

present only comparative results between circular and linear polarizations. In Fig. 3, the blue points are the six reference polarization states, the green points are the TN results, the yellow – FN and the red – TP, respectively. As can be seen from Fig. 3a and Fig. 3b, circular polarization holds better diagnostic opportunities than linear. Subtle to morphological alterations in tissues, when tumors are growing, the scattering of light will yield different polarization changes in the detected signal from different histological regions. Due to the higher tissue anisotropy of the intact zones, the initial circular polarization has been modified to linear. On the contrary, in the tumor sections of the sample, especially where the tumor has infiltrated at most, the output polarization state is closer to the initial. Nevertheless, in the regions with less tumor infiltration the output polarization states have contribution to the FN values. Positively, with both polarizations we do not have FP measurements (i.e. FP=0) and to our avail there are 36 TN values from the scans of both histological sections. Unfortunately, the use of horizontal polarization for the incident light does not provide TP results. With circular polarization we were able to detect 22 from 36 FN, where only for the latter polarization state the TP results are available – 14 from 36. The above-mentioned diagnostic quantities are summarized in the Table 1 for both input polarization states and both histological zones of the tissue.

[%]	Sens.	Spec.	Acc.	PPV	NPV	IS	TS
RCP	39	100	70	100	62	39	39
H	0	100	50	0	50	0	0

TABLE 1 Diagnostic quantities for both scanning polarizations.

3.2 | Statistical analysis

In this subsection we present the results from the statistical analysis, described in the Materials and Methods section earlier. In Fig.3a, it was shown that it is possible to differentiate with input circular polarization qualitatively between healthy and tumor tissues, depending on polarization states changes, traceable on the Poincaré sphere. On the contrary, this is not valid for linear polarization in Fig. 3b. Thus, Mann-Whitney U test served only for linear polarization to compare S_{TNi} vs S_{FNi} values, where $i = 1,2,3$. Tests' results indicate no significance difference between the compared values, decision taken on a significance level 0.05. Since we have TP values solely when a scan with circular polarization was made, therefore in that
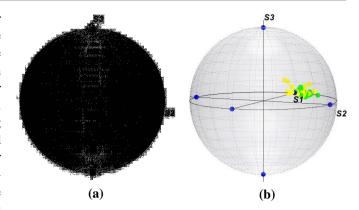

FIGURE 3 Distribution of the Stokes parameters on the Poincaré sphere, regarding the histological condition and input polarization: (a) input circular polarization and (b) input horizontal polarization. ● – representing six reference polarization states (H, V, P/MP, R/LCP), ● – TN values (36 for both polarization states), ● – FN values (36 for linear polarization and 22 for circular polarization), ● – TP values (14 available only for circular polarization). Total number of measurements – 36.
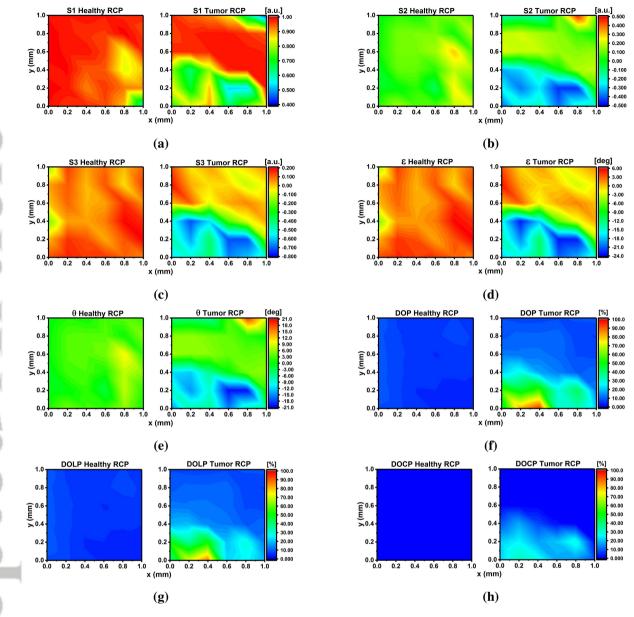
event should the Kruskal-Wallis test be performed. In this case, the comparison is for S_{TNi} vs S_{FNi} vs S_{FNi} values, where tests' results indicated, that on a confidence level 0.05 there is a significance difference between groups. Knowledge whether the values within the groups are drawn from the same or distinct populations can be provided by the omnibus *post-hoc* analysis associated with Tukey's test. The results suggest for $\alpha = 0.05$, that S_{FNi} vs S_{TPi}, S_{TNi} vs S_{TPi} and $S_{TN2,3}$ vs $S_{FN2,3}$ values are from different populations, omitting only S_{TN1} vs S_{FN1}.

3.3 | 2D polarimetric mapping

In this subsection we present results from the performed scanning of the colon sample's ROIs. By this approach, we aim to map any alterations in the polarimetric parameters from Eq. 1 through Eq. 4, measured with circular and linear polarizations and to relate their behaviour, according to the histological condition of the scanned area. The data was processed with OriginLab, whereas the plotting was chosen as contour fill with additionally applied liner interpolation between data points.
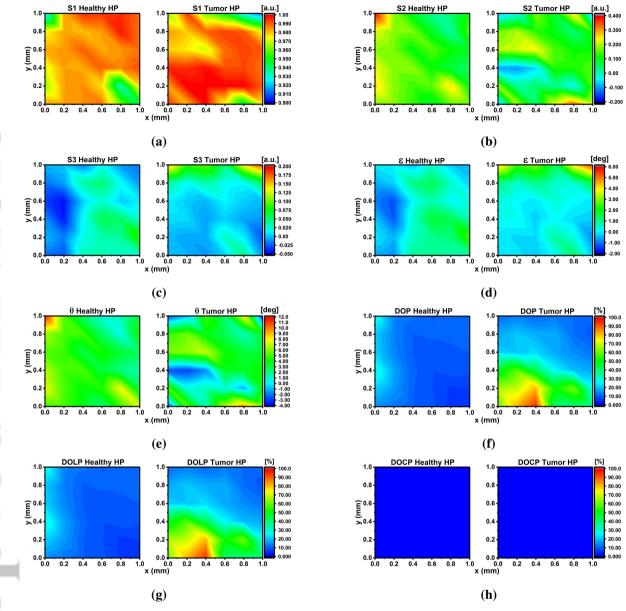
3.3.1 | Scanning with circular polarization

To begin with, right circular polarization can be characterized by its Stokes vector $S_{RCP}=(1,0,0,1)^T$ and the ellipticity angle 45°, while the azimuth is undefined. It can be seen from Fig. 4, that after the scan both sample sections change by different way the Stokes parameters. For example, in the healthy section circular polarization has been transformed into horizontal, while in the tumor section where the tumor has infiltrated at most,

FIGURE 4 2D polarimetric parameters mapping of both ROIs with circular polarization, depending on the histological condition: (a) S_1, (b) S_2, (c) S_3, (d) angle of ellipticity, (e) azimuth, (f) DOP, (g) DOLP, (h) DOCP.

we have closer values of the Stokes parameters to the initial and the detected output polarization is elliptical. Another confirmation of this phenomena can be traced back to the Poincaré sphere in Fig. 3a and the corresponding clusters of TP, TN and FN values. Comparing the spatial distribution of the ellipticity and azimuth angles we again confirm the milder polarization changes in the tumor section. At this stage we should outline, despite the fact that for input circular polarization the azimuth is not defined, when analysing elliptical polarization as in the current case, the azimuth angle can be reconsidered diagnostically. And finally, resolving all DOPs leads us to

the conclusion, that tumor zones can retain higher degree of polarization, compared to the healthy ones. It should be also pointed out, that the initial handedness of the circular polarization was right, however, some of the polarimetric parameters from the tumor tissue measurements indicate left handedness. This is unique property of helicity flip of light with circular/elliptical polarization, resulting from reflection or multiple reflections.[39]

FIGURE 5 2D polarimetric parameters mapping of both ROIs with linear polarization, depending on the histological condition: (a) S_1, (b) S_2, (c) S_3, (d) angle of ellipticity, (e) azimuth, (f) DOP, (g) DOLP, (h) DOCP.

3.3.2 | Scanning with linear polarization

Analogously to circular polarization, we can classify horizontal polarization with the following Stokes vector $\mathbf{S}_{HP}=(1,1,0,0)^{\mathbf{T}}$, azimuth 0° and angle of ellipticity 0°. However, unlike circular polarization, linear cannot provide such diagnostic capabilities in terms of polarization alterations, especially noticeable in Fig. 3b, where we have only TN and FN. The dynamic ranges of all polarimetric values for both histological sections except for DOP are lower for linear polarization, which also restricts the diagnostic opportunities.

In the cases of all DOPs, linear polarization compared to circular, retains higher values in turbid media such as biological tissues. This becomes evident from Fig. 4 and Fig. 5(f-h).

4 | CONCLUSIONS

In this paper combined polarimetric techniques have been described and used. The aim is to support any diagnostic conclusions of the "Gold Standard". Circular polarization was evaluated as more sensitive to tissue alterations, with a higher

dynamic ranges of the polarimatric quantities and in general as better for diagnostics with regard to linear. Furthermore, when scan with circular polarization was performed certain DOLP was sustained, whereas on the contrary, no DOCP was preserved when scanned with linear polarization. Moreover, the depolarization of circular polarization is higher with regard to liner polarization, forasmuch as depolarization behaviour of light in turbid media is strongly dependent on the scatters size, wavelength of the incident light and the transport parameters for any of the two histological zones. Our results validate both the assumption of Rayleigh scattering regime and the lesser tissue anisotropy of the tumor sections. Nevertheless, any polarization changes originating from different histological condition of the examined ROIs, can be traced qualitatively on the Poincaré sphere. Quantitatively, these changes can be evaluated in comparison with the help of the two-dimensional scanning and the resulting alterations in the polarimetric parameters described in the theoretical section. The spatial distribution of the polarimetric quantities can provide insight of small but significant morphological changes within the scanned area. In a significant addition to the Poincaré sphere representation, only with circular polarization we were able to detect TP values, crucial for diagnostics. What excels in a higher degree the better applicability of RCP can be revealed by the conducted statistical analysis. On a significance level $\alpha=0.05$ we can conclude, that with linear polarization our method is insensitive to TP values as well as contrasting between TN and FN values. Also, increasing importance can be added with regard to the diagnostic quantities calculated for both polarizations, which are either higher or non-zero in favor of RCP. Thus, this combined polarimetric approach on all sequential basis has a potential to separate healthy tissues from cancerous and/or precancerous and can be additionally characterized by the above-mentioned diagnostic techniques, relying entirely on a physical background. Although the Sensitivity, IS and TS have room for improvement, the Accuracy and NPV are well satisfactory, while the Specificity and the PPV are excellent, even for a pilot study. Two more steps can be assessed: *i)* To have better resolution between TN, FN and TP values by applying SVM and/or Regression analysis; *ii)* To enrich the polarimetric approach by using the measured Stokes parameters for obtaining the Mueller matrices of both histological sections under examination with primary focus on applying symmetric matrix decompositions. However, the former and the latter steps are beyond the scope of the current study and subsequently require more detailed review. Therefore, they will be thoroughly presented in further reports. Finally, our conclusion can be extended in a brief comparison with results obtained from various groups in the field of tissue polarimetry, whereas Sridhad *et al.* [49] achieved better sensitivity, higher contrast and signal intensity for 633 nm with

elliptical polarization than linear. Another important study in the NIR spectral region in terms of Mueller-matrix imaging spectroscopy by Wang *et al.* [50] unambiguously presents lesser depolarization coefficient for colonic cancer, while Zaffar *et al.* [51] utilized Poincaré sphere representation in order to differ between pre-cancerous and normal tissues.

ACKNOWLEDGMENTS

Financial disclosure

No financial conflicts or otherwise are declared by the authors.

Conflict of interest

The authors declare no potential conflict of interests.

References

[1] International Agency for Research on Cancer, *Global Cancer Observatory*, **2019**, Available from: http://gco. iarc.fr [last accessed: April 2020].

[2] M. Arnold, M. Sierra, M. Laversanne, I. Soerjomataram, A. Jemal, F. Bray, *GUT* **2017**, *66*, 683–691.

[3] S. Edge, *American Joint Committee on Cancer (AJC12) 6th ed.*, Springer, Chicago, **2002**.

[4] A. Pierangelo, S. Manhas, A. Benali, C. Fallet, J. Totobenazara, M. Antonelli, T. Novikova, B. Gayet, A. Martino, P. Validire, *J. Biomed. Opt.* **2013**, *18(4)*, 046014.

[5] C. Day, *Histopathology. Methods and Protocols 1st ed.*, Humana Press, New Jersey, **2014**.
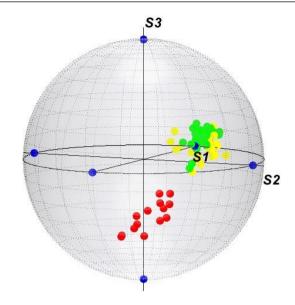
[6] D. Wittekind, *J. Biotechnic. and Histochemistry* **2003**, *78(5)*, 261–270.

[7] H. Wei, D. Xing, J. Lu, H. Gu, Y. Wu, G. amd Jin, *World J. Gastroenterol.* **2005**, *11(6)*, 2413–2419.

[8] M. D. Beswick, A. Kaushik, D. Beinart, S. McGarry, M. K. Yew, F. B. Kennedy, S. L. P. Maria, *J. Biomed. Opt.* **2018**, *23(2)*, 021102.

[9] L. Marcu, A. S. Boppart, R. M Hutchinson, J. Popp, C. B. Wilson, *J. Biomed. Opt.* **2018**, *23(2)*, 021103.

[10] Ts. Genova, E. Borisova, N. Penkov, B. Vladimirov, A. Zhelyazkova, Avramov L., *Quant. Electr.* **2016**, *46(6)*, 510–514.

[11] L. Liu, Y. Nie, L. Lin, W. Li, Z. Huang, S. Xie, B. Li, *Photodiagn. Photodyn. Ther.* **2012**, *10(2)*, 111–119.

[12] M. Nakamura, A. Goto, A. Nishikawa, H. Shibata, *World J. Gastroenterol.* **2015**, *21(21)*, 6706–6712.

[13] E. J. M. Baltussen, P. Snaebjornsson, S. G. Brouwer de Koning, H. J. C. M. Sterenborg, A. G. J. Aalbers, N. Kok, G. L. Beets, B. H. W. Hendriks, K. F. D. Kuhlmann, T. J. M. Ruers, *J. Biomed. Opt.* **2017**, *22(10)*, 106014.

[14] C. A. Jenkins, P. D. Lewis, P. R. Dunstan, D. A. Harris, *World J. Gastrointest. Oncol.* **2016**, *8(5)*, 427–438.

[15] H. Chen, Z. Lin, L. Mo, T. Wu, C. Tan, *Biomed. Res. Int.* **2015**, *2015*, 1–8.

[16] P. C. Ashok, B. B. Praveen, N. Bellini, A. Riches, K. Dholakia, S. Herrington, *Biomed. Opt. Express* **2013**, *4(10)*, 2179–2186.

[17] L. Ehlen, U. J. Zabarylo, F. Speichinger, A. Bogomolov, V. Belikova, O. Bibikova, V. Artyushenko, O. Minet, K. Beyer, M. E. Kreis, C. Kamphues, *J. Surg. Res.* **2019**, *242*, 349–356.

[18] V. Subramanian, K. Ragunath, *Clin. Gastroenterol. Hepatol.* **2014**, *12(3)*, 368–376.

[19] M. Alam, S. Vedaei, K. Wahid, *Cancers* **2020**, *12*, 890.

[20] T. Novikova, I. Meglinski, J. Ramella-Roman, V. Tuchin, *J. Biomed. Opt.* **2016**, *21* (7), 071001.

[21] D. Ivanov, R. Ossikovski, T. Novikova, P. Li, B. Borisova, T. Genova, L. Nedelchev, D. Nazarova, *Proc. SPIE* **2019**, *11075*, 1107514.

[22] D. Ivanov, T. Genova, E. Borisova, L. Nedelchev, D. Nazarova, *Proc. SPIE* **2019**, *11047*, 1104707.

[23] D. Ivanov, E. Borisova, T. Genova, L. Nedelchev, D. Nazarova, *AIP Conference Proceedings.* **2019**, *2075*, 170017.

[24] V. Ushenko, A. Sdobnov, A. Syvokorovskaya, A. Dubolazov, O. Vanchulyak, A. Ushenko, Y. Ushenko, M. Gorsky, M. Sidor, A. Bykov, I. Meglinski, *Photonics* **2018**, *5*, 54.

[25] M. Borovkova, V. A. Ushenko, A. V. Dubolazov, O. Ya. Vanchulyak, O. G. Ushenko, A. V. Bykov, I. Meglinski, *PLOS One* **2019**, *14* (5), e0214494.

[26] N. K. Das, S. Chakraborty, R. Dey, P.K. Panigrahi, I. Meglinski, N. Ghosh, *Opt. Commun.* **2018**, *413*, 172 – 178.

[27] A. Ushenko, A. A. Sdobnov, Dubolazov, M. Gritsuk, Y. Ushenko, A. Bykov, I. Meglinski, *IEEE J. Sel. Top. Quantum Electron.* **2019**, *25* (1), 7101612.

[28] V. Dremin, D. Anin, O. Sieryi, M. Borovkova, J. Näpänkangas, I. Meglinski, A. Bykov, *Proc. SPIE* **2020**, *11363*, 1136304.

[29] S. Manhas, K. M. Swami, S. H. Patel, A. Uppal, N. Ghosh, P. K. Gupta, *J. Biophotonics* **2009**, *2*, 581–587.

[30] A. Pierangelo, S. Manhas, A. Benali, C. Fallet, J. Totobenazara, R. M. Antonelli, T. Novikova, B. Gayet, A. Martino, P. Validire, *J. Biomed. Opt.* **2012**, *17*, 066009–1–6.

[31] A. Pierangelo, A. Benali, C. Fallet, M. Antonelli, T. Novikova, P. Validire, B. Gayet, A. Martino, *Biomed. Opt. Express* **2011**, *19*, 1582–1593.

[32] M. Borovkova, M. Peyvasteh, Y. O. Ushenko, O. V. Dubolazov, V. O. Ushenko, A. V. Bykov, T. P. Novikova, I. Meglinski, *J. Eur. Opt. Soc.-Rapid.* **2018**, *14*, 20.

[33] C. Macdonald, I. Meglinski, *Laser Phys. Lett.* **2011**, *8* (4), 324.

[34] I. Meglinski, C. Macdonald, K. Anthony, H. Yoon, M. Eccles, in *Biomedical Optics, OSA Technical Digest*, **2012**, p. BW3B.6.

[35] I. Meglinski, C. Macdonald, A. Doronin, M. Eccles, in *Optics in the Life Sciences, OSA Technical Digest (online)*, **2013**, p. BM2A.4.

[36] B. Kunnen, C. Macdonald, A. Doronin, S. Jacques, M. Eccles, I. Meglinski, *J. Biophotonics* **2015**, *8*, 317–323.

[37] R. C. Jones, *J. Opt. Soc. Am.* **1947**, *37*, 107–110.

[38] R.M.A. Azzam, N.M. Bashara, *Ellipsometry and polarized light*, Amsterdam, North-Holland, **1977**.

[39] D. H. Goldstein, *Polarized Light - Third edition*, CRC Press, Taylor and Francis, **2010**.

[40] V-D. Tuan, *Biomedical Photonics Handbook*, CRC Press, New Work, **2003**.

[41] R Core Team, *R: A Language and Environment for Statistical Computing*, R Foundation for Statistical Computing, Vienna, Austria, **2017**. https://www.R-project.org/.

[42] M. Borovkova, A. P. Popov, A. V. Bykov, I. Meglinski, *J. Biomed. Opt.* **2020**, *XX* (x), in press.

[43] M. Xu, R.R. Alfano, *Phys. Rev. E* **2005**, *72* (6), 065601.

[44] F.C. MacKintosh, J.X. Zhu, D.J. Pine, D.A. Weitz, *Phys. Rev. B* **1989**, *40* (13), 9342.

[45] V.L. Kuzmin, Meglinski I., *Proc. SPIE* **2010**, *7573*, 75730Z.

[46] V.L. Kuzmin, Meglinski I., *J. Exp. Theor. Phys.* **2010**, *110* (5), 742–753.

[47] W. Wang, G.L. Lee, S. Supriya, J.S.B. Yan, A. Shabbir, L. Quan, *J. Biomed. Opt.* **2014**, *19*, 046020–1–10.

[48] C. Macdonald, A. Doronin, A.F. Pena, M. Eccles, I. Meglinski, *Proc. SPIE* **2014**, *8940*, 894007.

[49] S. Susmita, A. Da Silva, *J. Biomed. Opt.* **2016**, *21(7)*, 071107.

[50] J. Wang, W. Zheng, K. Lin, Z. Huang, *Biomed. Opt. Express* **2016**, *7(4)*, 1116–1126.

[51] M. Zaffar, M.A. Pradhan, *J. Biophotonics* **2020**, *e201960139*.

How to cite this article: D. Ivanov , V. Dremin, A. Bykov, E. Borisova, T. Genova, A. Popov, R. Ossikovski, T. Novikova and I. Meglinski (2020), Colon cancer detection via Poincaré sphere representation and 2D polarimetric mapping of *ex vivo* colon sample, *J. Biophotonics*, *20XX;XX:X*.

GRAPHICAL ABSTRACT

Polarization of light can be exploited in cancer detection and can enrich physicians diagnostics. The Stokes-Mueller formalism as well as Poincaré sphere representation are essentials in turbid media, which retain arbitrary degree of the input polarized light. Such approach holds promises for *in vivo* cancer detection with no ionizing radiation or any toxic agents in use.